Observation of the transition from image-potential states to resonances on argon-covered Cu(111) and Ag(111) by time-resolved two-photon photoemission

A. Damm, K. Schubert, J. Güdde, and U. Höfer
Fachbereich Physik und Zentrum für Materialwissenschaften, Philipps-Universität, D-35032 Marburg, Germany
(Received 17 July 2009; revised manuscript received 23 October 2009; published 25 November 2009)

The influence of well-ordered adlayers of Argon on binding energies and inelastic lifetimes of image-potential states and resonances on Cu(111) and Ag(111) has been investigated by means of time-resolved two-photon photoemission spectroscopy. The adsorption of Ar layers on metals results in a strong decoupling of the image-potential states that goes along with an exponential increase in their inelastic lifetimes and a lowering of their binding energies. The latter shifts the first ($n=1$) image-potential state above the minimum of unoccupied projected bulk bands on Cu(111) and thereby induces a transition from an image-potential state to a resonance. This leads to a strikingly different dependence of the inelastic lifetime of the $n=1$ state on Ar layer thickness for the two surfaces. On Ag(111) the lifetime shows a continuous exponential increase with layer thickness from 32 fs on the clean surface to about 6 ps for an Ar coverage of four monolayers (ML). On Cu(111) the exponential increase is considerably reduced when the $n=1$ state becomes a resonance. Up to 10 ML of Ar the lifetime on Cu(111) does not exceed 3 ps. This rather unexpected behavior can neither be explained by a simple tunneling picture of the tunneling through thin Ar films nor by model calculations using a one-dimensional model potential that accounts for the most important electronic properties of both the metal substrate as well as of the Ar layers.

DOI: 10.1103/PhysRevB.80.205425 PACS number(s): 73.20.−r, 73.40.Ns, 78.47.J−, 79.60.−i

I. INTRODUCTION

Femtosecond time-resolved two-photon photoemission (2PPE) has become a very versatile and successful technique to study ultrafast electron dynamics at surfaces and interfaces.[1–11] On metal surfaces in particular, the investigation of image-potential states has led to a rather detailed understanding of the many-body processes, which are responsible for the inelastic decay of electronic excitations.[12–15] Recent progress includes studies of lateral, quasielastic scattering processes,[16–18] the spectroscopy of buried interface states,[19] and the observation of spin-dependent electron dynamics[20] and of optical spin injection.[21] The hydrogenlike image-potential states are typically confined in front of the surface by the attractive image force on the vacuum side and a forbidden gap in the band structure on the substrate side. Therefore, the energy of these states is usually located within the projected bulk band gap, which limits the penetration of the excited electrons into the bulk.[22] In many systems or surface phenomena that are connected to electron transfer, however, electronic resonances, i.e. electronic states at the surface that are resonant with bulk states, play an important role. So far, however, only a few experimental as well as theoretical efforts have been made to improve the understanding of electron dynamics of resonant charge transfer at interfaces.[23–26] These works have shown that resonant charge transfer into the bulk is often more efficient than inelastic decay of the excited electrons.

In this contribution we show that the adsorption of well-ordered rare-gas layers can be used to change the character of image-potential states on a metal surface from surface states (SSs) to surface resonances, which makes it possible to study the influence of resonant charge transfer on the dynamics of these surface states. For this purpose we have investigated the influence of well-ordered Argon layers on the energies and inelastic lifetime of image-potential states on the (111) surfaces of Cu and Ag using time- and angle-resolved 2PPE. In contrast to the (100) noble-metal surfaces, where the image-potential states are located in the center of the surface projected bulk band gap, the image-potential states on the (111) noble-metal surfaces are close to the edge of an unoccupied projected bulk band. Therefore, even a slight modification of the binding energy of the image-potential states can tune them into resonance with the projected bulk band.

From experiments performed over the past years it is known that, for adsorbates which do not introduce additional unoccupied electronic levels in the energy range of the image-potential states, the latter will retain their simple hydrogenic character but will be repelled from the metal.[27–37] This decoupling of the image-potential states goes along with an increase in their inelastic lifetime as well as with a reduction in their binding energies with respect to the vacuum level. The strength of the decoupling is mainly determined by the electron affinity of the adsorbate film and the layer thickness.[37] For rare gases with negative electron affinity, like in the case of Ar, the insulating film represents an efficient tunnel barrier for image-potential states, which results in an exceptionally strong decoupling. For Ar/Cu(100), for example, it has been found that the inelastic lifetime of the first ($n=1$) image-potential state increases exponentially from 40 fs on the clean surface up to 10 ps at a thickness of five monolayers (ML).[35–40]

It will be shown that, although the electronic properties of the (111) surfaces of Cu and Ag are very similar, slight differences in the decoupling of image-potential states upon Ar adsorption result in completely different dynamics of the $n=1$ state on these surfaces. While on Cu(111) $n=1$ shifts above the projected bulk band minimum, it remains in the projected bulk band gap on Ag(111). The transition from a

bound state to a resonance on Cu(111) is found to be directly reflected in the inelastic lifetime of electrons optically excited in these states. When the $n=1$ state becomes resonant to the projected Cu bulk band, the slope of the exponential increase in the lifetime is reduced. While the exponential increase in the lifetime with Ar coverage can be understood in a simple tunneling picture, the change in the slope for image-potential resonances compared to image-potential states is unexpected and cannot be satisfactorily described within the framework of current models.

The paper is organized as follows. The next section gives a brief description of the experimental setup and the preparation of well-ordered Ar layers. The focus of the third section lies on the change in work function as well as in the binding energies of the image-potential states and resonances upon Ar adsorption. The fourth section presents the experimental results on the coverage dependence of the lifetimes, which is followed by a discussion of these results within a simple tunneling picture as well as on the basis of model calculations using a one-dimensional parametrized potential for rare-gas covered metal surfaces.

II. EXPERIMENT

The experiments were carried out in an ultrahigh vacuum chamber with a base pressure of better than 5×10^{-11} mbar at room temperature. A Cu(111) single crystal with an orientation accuracy of better than 0.25° and an Ag(111) single crystal with an orientation accuracy of better than 0.1° were used. The samples were attached to a liquid-helium cryostat and could be cooled down to 25 K. Sample preparation consisted of standard sputter-annealing cycles. Surface cleanliness and order were verified by x-ray photoelectron spectroscopy, low-energy electron diffraction, and linewidth measurements with 2PPE.[41] Photoelectrons emitted from the sample were detected by a hemispherical electron analyzer (Specs Phoibos 150) equipped with a two-dimensional (2D) charge-coupled-device detector and an angle-resolved lens mode.[42] The energy and momentum resolutions have been determined to be 14 meV and 0.005 $Å^{-1}$, respectively. Energy-resolved spectra were obtained from cuts of the 2D spectra with a width of about 0.035 $Å^{-1}$ (20 pixels).

Well-ordered Ar adlayers of controlled thickness were prepared by adsorbing Ar on top of an annealed Ar monolayer.[35] For this purpose the sample was exposed to a homogeneous Ar flux of a microcapillar doser. The first monolayer has been prepared by dosing an amount exceeding 1 ML followed by annealing the sample to a temperature just below the onset of desorption from the first monolayer. Coverage calibration has been done by exploiting the zeroth-order desorption kinetics of rare gases in high-resolution temperature-programmed desorption (TPD).[43] Figure 1 shows TPD spectra for different coverages of Ar on Cu(111) and Ag(111) grown on an annealed monolayer. The sharp and well-separated peaks for 1, 2, and 3 ML demonstrate layer-by-layer desorption of the films. The small temperature difference in the fall of the first ML peak between Cu(111) and Ag(111) indicates that the first monolayer of Ar is slightly stronger bound on Ag(111) compared to Cu(111).

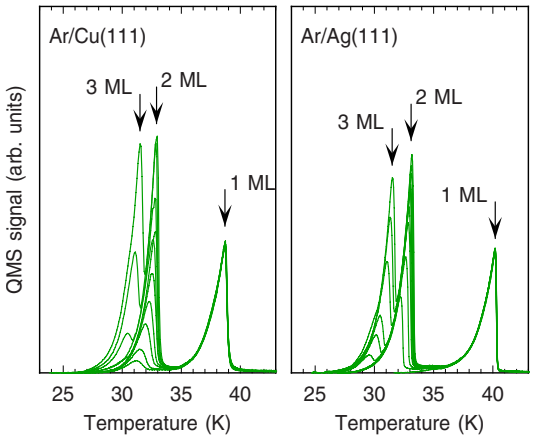

FIG. 1. (Color online) Temperature programmed desorption (TPD) spectra of Ar adsorbed on Cu(111) (left) and Ag(111) (right). Multilayers were grown on top of an annealed monolayer. The sharp peaks indicate the growth of highly ordered layers.

The optical setup for the 2PPE measurements consists of a femtosecond Ti:sapphire laser amplifier system (Coherent RegA) operating at 800 nm with a repetition rate of 100 kHz that generates 60 fs laser pulses with a pulse energy of 6 μJ. The output of the amplifier is used to pump a traveling-wave optical parametric amplifier that produces laser pulses in the visible range with a pulse length of typically 50 fs [full width at half maximum (FWHM)]. For the experiments on Cu(111) and Ag(111) the wavelength was chosen between 515 and 580 nm in order to account for the different work functions of the samples. The pulse energy has been adjusted between 50 and 200 nJ. The dispersion of these pulses in the optical elements of the setup was compensated by a prism compressor consisting of a pair of $LaFN_{28}$ Brewster prisms. Laser pulses in the ultraviolet, which served as pump pulses with frequency ω_a, were generated by frequency doubling of the visible pulses (frequency $\omega_a/2$) in a type I phase-matched β-barium borat (BBO) crystal with a thickness of 100 μm. A part of the fundamental laser beam served as probe pulses and could be time delayed by a motor-driven delay stage with a resolution of better than 1 fs.

Figure 2 shows raw two-dimensional $E(k_\parallel)$ spectra for 3 ML of Ar/Cu(111). The left spectrum has been taken at temporal overlap between pump and probe laser pulses. It is clearly dominated by the nonresonant two-photon photoemission signal of the Shockley SS. In the right spectrum, which has been taken at a time delay between pump and probe pulses of about 200 fs, the signal of the Shockley surface state is vanished, but the photoemission signals of the $n=1$ and 2 image-potential bands are now clearly visible. As a relict of the Shockley state, the photoemission signal is enhanced at those points in the band structure where the SS is resonant with the image-potential bands.

III. ENERGIES

In photoemission experiments energies of electronic states are typically given with respect to the Fermi level E_F, which is the intrinsic reference level of the bulk system. This en-

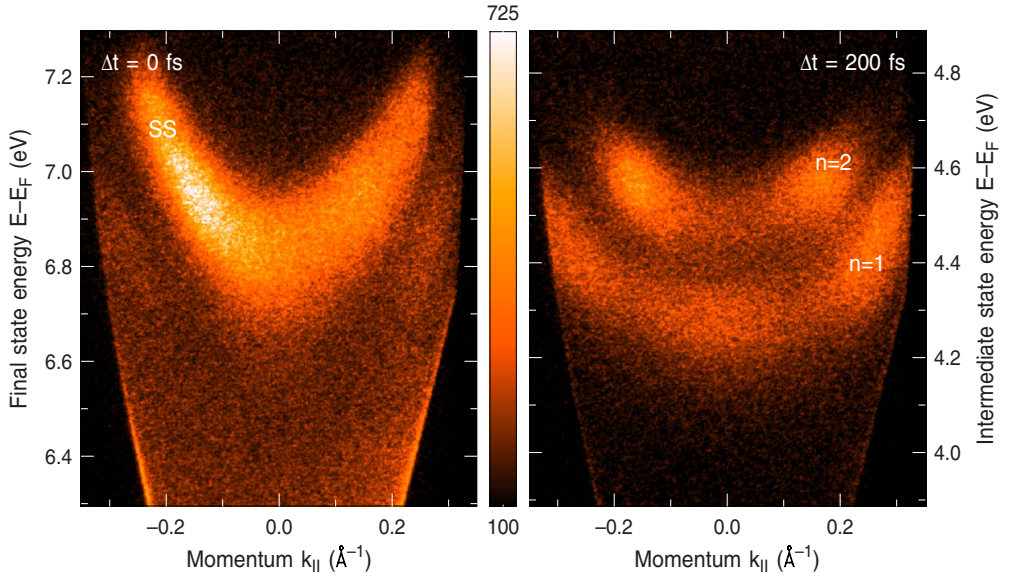

FIG. 2. (Color online) Two-dimensional $E(k_{\|})$ spectra of 3 ML Ar/Cu(111) for a time delay between pump and probe pulses near zero (left) and at about 200 fs. The energy is given as the energy of the final state with respect to the Fermi energy E_F on the left side and as the energy of the intermediate state on the right side. Thus, the two energy scales differ by the photon energy of the probe pulse $\hbar\omega_a$. (Note that the Shockley surface state is nonresonantly photoemitted in a two-photon process without a real intermediate state.) The color bar in the middle denotes the intensity scale of the 2D spectra. While for small delays Δt the nonresonant 2PPE signal of the Shockley surface state (SS) dominates the photoemission spectra, the $n=1$ and 2 image-potential bands are most prominent for larger delays.

ergy can be determined independent of the actual difference between the work function Φ of the sample and the electron energy analyzer by measuring the kinetic energy of the photoemitted electrons with respect to the high-energy cutoff of the photoemission spectra, which is the photoemitted replica of the Fermi edge. Image-potential states, however, form a Rydberg-like series of states at the surface that converges to the vacuum level E_{vac}. Therefore, their natural reference level is represented by E_{vac} rather than by E_F. In principle their energy with respect to E_{vac} can be determined by measuring the kinetic energy of the photoemitted electrons from the 2PPE spectrum with respect to the onset of the low-energy cutoff of the single photon photoemission spectrum and subtracting the photon energy of the photoemitting laser pulse. The low-energy cutoff corresponds to electrons excited by the pump pulse that just can overcome the work function of the sample if the latter is larger than that of the electron energy analyzer. This procedure, however, depends sensitively on the definition of the onset of the low-energy cutoff. This is one reason why we have determined the energies of the image-potential states in a different way as described below. The other more important reason is the fact that the dynamics of the image-potential states on the Ar covered Cu(111) and Ag(111) surfaces depend primarily on their energetic position with respect to the bulk electronic structure and not on their binding energy relative to the (varying) vacuum level. Therefore, the low-energy cutoff has been used here only to determine the change in the work function with Ar coverage. The left part of Fig. 3 shows the low-energy cutoff of the photoemission spectra for the clean and Ar-covered Ag(111) recorded in normal emission for a UV photon energy of $\hbar\omega_a=4.92$ eV, which is larger than the work function of the clean Ag(111) surface of $\Phi=4.56$ eV.[44] Clearly the low-energy cutoff shifts to lower energies with Ar coverage. In contrast to the onset, the relative shift of the cutoff, which directly represents the change in the work function $\Delta\Phi$, can be determined with an accuracy of better than 10 meV. As indicated by the vertical bars in Fig. 3 the work function of Ag(111) changes by $\Delta\Phi=-280$ meV upon adsorption of the first monolayer of Ar and saturates for coverages $\theta\geq 3$ ML at $\Delta\Phi=-300$ meV (cf. Table I), which corresponds to an absolute value of $\Phi=4.26$ eV. On Cu(111) the drop of the work function by Ar adlayers is slightly smaller and saturates for coverages $\theta\geq 4$ ML at $\Delta\Phi=-280$ meV, which corresponds to $\Phi=4.59$ eV.

The energies of the image-potential states with respect to E_F have been determined by measuring the kinetic energy of the photoemitted electrons with respect to the signal of nonresonant 2PPE from the occupied Shockley state (SS), which is shown in the middle part of Fig. 3. The energy of this state with respect to E_F has been measured by high-resolution single-photon photoemission spectroscopy for the clean (111) surfaces of Ag, Cu, and Au (Ref. 45) and for 1 ML of Ar, Kr, and Xe.[46] For Ag(111) it shifts from $E_{SS}-E_F=-62$ meV on the clean surface toward the Fermi level ($E_{SS}-E_F\approx 0$ meV) for 1 ML of Ar. This is in very good agreement with our results as shown in the middle part of Fig. 3. For higher Ar coverages no further shift of the energy has been observed. The same behavior has been found for Cu(111) where the energy shifts from $E_{SS}-E_F=-434$ meV for the clean surface to $E_{SS}-E_F=-376$ meV for the Ar covered surface. The energies of the image-potential states on the clean Cu(111) surface with respect to E_{vac} have been determined from their energies with respect to E_F and the work function of $\Phi=4.87$ eV as reported in Refs. 44 and 47. The binding energies obtained in this way are in good agree-

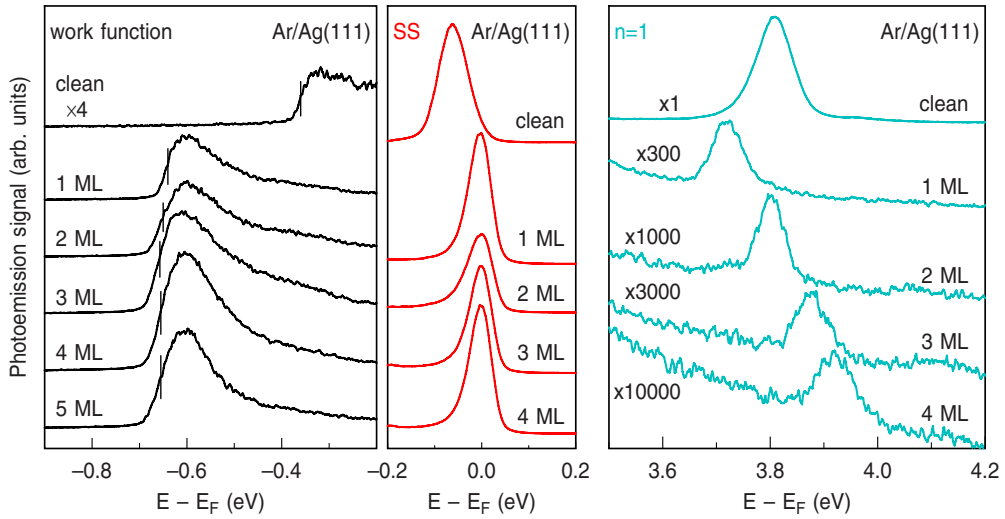

FIG. 3. (Color online) Details of photoemission spectra recorded in normal emission for different Ar coverages on Ag(111). Left: vacuum edge by direct photoemission by the uv-pump pulses. Middle: nonresonant two-photon photoemission of the Shockley SS. Right: two-photon photoemission of the first ($n=1$) image-potential state.

ment with those reported in the literature.[14,44] The energies of the image-potential states on the clean Ag(111) surface with respect to E_{vac} have been determined in a different experiment by fitting the peak positions of the image-potential states to a Rydberg series, $E_n=E_{vac}-0.85\ \text{eV}/(n+a)^2$.[48] The change in the binding energies of the image-potential states (with respect to E_{vac}) with Ar coverage has been determined from the change in their energies with respect to E_F and the change in the work function $\Delta\Phi$.

The right part of Fig. 3 shows 2PPE spectra of the $n=1$ image-potential state on Ag(111) for Ar coverages of 0–4 ML. For these spectra the photon energy of the exciting pump laser pulses was adjusted to $\hbar\omega_a=4.27$ eV significantly below the work function of the clean Ag(111) surface in order to reduce the background from one-photon photoemission. Therefore, only the first image-potential state can be populated on the clean surface. For the Ar covered surface the same photon energy is sufficient to populate also higher image-potential states due to the reduced work function. In this case, however, the lower signal-to-noise ratio (S/N) prevented the observation of the image-potential states with higher quantum number n. On the Ar covered Ag(111) surface the maximum achievable S/N was limited by laser-induced desorption of Ar due to the visible probe laser beam. A similar process has already been observed for Ar/Cu(100).[49] This process, however, is much more efficient for Ar/Ag(111). For this reason it was necessary to keep the laser intensity low that also has limited the accessible range of Ar coverages. For Cu(111), on the contrary, no laser-induced desorption has been observed and the usable laser intensity was only limited by space-charge effects that become noticeable by an intensity-dependent shift of the 2PPE spectrum. The corresponding data for 0–5 ML of Ar/Cu(111) are shown in Fig. 4. In addition to the signal from the $n=1$ image-potential state a clear signal from $n=2$ can be observed. With increasing coverage both states lose binding energy with respect to E_{vac}, but only $n=1$ shifts upward in energy with respect to E_F. $n=2$ shifts down with respect to E_F since the drop of its binding energy is smaller than the drop of the work function. All the spectra shown in Figs. 3 and 4 have been scaled in order to get a comparable intensity of the 2PPE signal. The scaling factor denoted on the left side of each spectrum is thus a measure of the 2PPE signal intensity of the $n=1$ state. For Ag(111) the signal intensity decreases by four orders of magnitude with increasing Ar coverage. This decrease is comparable to Ar/Cu(100). In contrast, Ar/Cu(111) exhibits a much weaker decrease in the signal intensity. This is a first indication that the decoupling of the image-potential states by Ar adlayers is different for these two surfaces. The oscillatory behavior of the signal intensity as a function of Ar coverage observed for Cu(111) can be explained by a variation of the wave function overlap between the image and the final states of the photoemission process with Ar coverage.[35]

The decoupling of the image-potential states by the repulsive Ar layers results in a monotonous decrease in their binding energies with respect to the vacuum energy with Ar coverage on both investigated surfaces (Table I). The results on

TABLE I. Shift of the work function with respect to the clean surface ($\Delta\Phi$) and energy E_n of the $n=1,2$ image-potential states with respect to the vacuum level for different coverages θ of Ar on Cu(111) and Ag(111). All energies are given in meV and were determined at a sample temperature of $T_S\approx 26$ K.

θ	Ar/Cu(111)			Ar/Ag(111)		
(ML)	$\Delta\Phi$	$E_{n=1}$	$E_{n=2}$	$\Delta\Phi$	$E_{n=1}$	$E_{n=2}$
0	−0	−826	−250	−0	−751	−211
1	−240	−546	−178	−280	−584	
2	−265	−375	−125	−290	−493	
3	−275	−344	−111	−300	−408	
4	−280	−310	−97	−300	−369	
5	−280	−270	−90	−300		

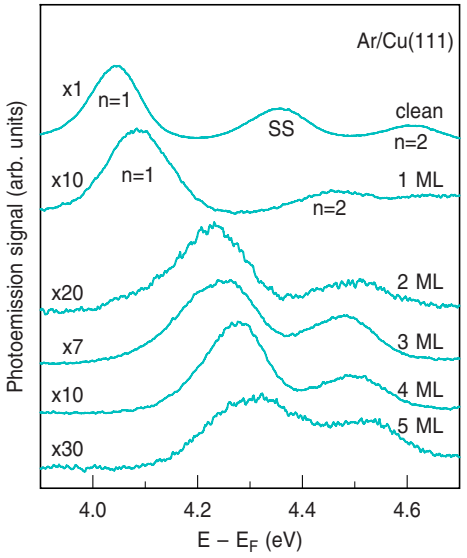

FIG. 4. (Color online) Energy-resolved 2PPE spectra of Ar/Cu(111) at the $\bar{\Gamma}$ point ($k_{\parallel}=0$) obtained from two-dimensional $E(k_{\parallel})$ spectra as shown in Fig. 2 for Ar coverages from 0–5 ML. The curve for the clean surface shows the spectrum for temporal overlapping pump and probe pulses where the Shockley SS is visible. All other curves show spectra at a time delay larger than the width of the cross correlation of pump and probe pulses in order to emphasize the signals of the image-potential states.

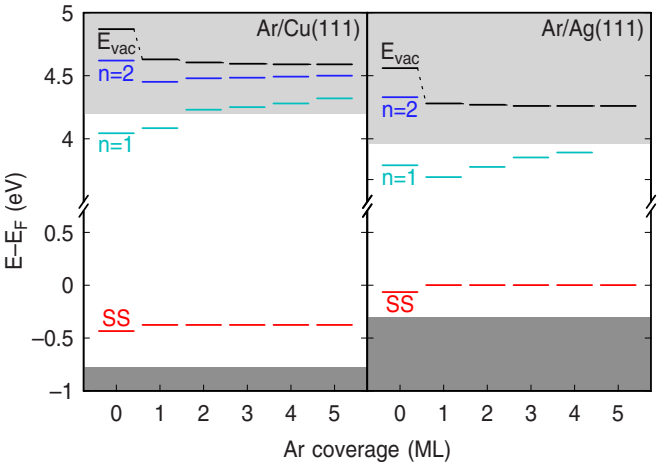

FIG. 5. (Color online) Energy diagram of the image-potential states on Ar/Cu(111) (left) and Ar/Ag(111) (right) at the $\bar{\Gamma}$ point for different Ar coverages summarizing the experimental results as obtained from 2PPE spectra similar to those shown in Figs. 3 and 4. All energies are given with respect to the Fermi level E_F. Horizontal lines represent the Shockley SS, the $n=1,2$ image potentials, and the vacuum energy (E_{vac}). The energies of the SS state have been taken from Refs. 45 and 46. The error of the determined energies is within the thickness of the lines. Shaded areas depict the projected bulk band structure. Dark areas correspond to the occupied valence band whereas light areas show the unoccupied projected bulk band.

the energies with respect to E_F for both surfaces are depicted in Fig. 5 as a function of Ar coverage together with the projected bulk band structure at the $\bar{\Gamma}$ point. Due to the initial drop of the work function upon Ar adsorption, the energy of the $n=1$ state with respect to E_F also drops for the first monolayer Ar on Ag(111), but then increases monotonously with increasing coverage. On Cu(111) the drop of the binding energy of the $n=1$ state with respect to E_{vac} exceeds the drop of the work function for all coverages. Therefore, its energy with respect to E_F and thus with respect to the bulk bands increases monotonously with coverage. The image-potential states with quantum numbers $n\geq 2$ are resonant with the projected bulk band on both surfaces and all Ar coverages. Therefore, these states are strictly spoken image-potential resonances. An optical excitation into these continuous bands creates wave packets that are only initially located at the surface, but which can decay into the bulk by motion of the wave packet perpendicular to the surface.[25] On the contrary, the $n=1$ state is, for low Ar coverages, located within the projected bulk band gap on both surfaces. On Cu(111) the $n=1$ state becomes resonant with the bulk band for Ar coverages of $\theta\geq 2$ ML whereas on Ag(111) it remains within the projected bulk band gap for a coverages of at least up to 4 ML. We stress again that the crossing of $n=1$ and the bulk band of Cu(111) is independent of any uncertainties in the determination of the work function because all energies were measured with respect to the Fermi level as described above.

IV. LIFETIMES

The decay of electrons optically excited into image-potential states has been observed by recording 2D photoemission spectra in normal emission as a function of delay between pump and probe pulses. Time-resolved pump-probe traces as shown in Fig. 6 for the $n=1$ state on clean and Ar covered Cu(111) (top) and Ag(111) (bottom) were obtained by integrating the photoemission intensity over an area with a width of 0.018 $Å^{-1}$ and a height of 33 meV (20 $\times$20 pixels) around the peak maxima at the $\bar{\Gamma}$ point. The dashed (black) line denotes the cross correlation of the pump and probe laser pulses obtained by recording the nonresonant two-photon photoemission of the Shockley surface state. The length of pump and probe pulses was determined to be in both cases typically shorter than 60 fs. For pump-probe delays that are larger than the width of the cross correlation, the data on both surfaces show a pure exponential decay that slows down with increasing Ar coverage. In contrast to the data on Ag(111), the data on Cu(111) show a pronounced narrow peak around zero delay. This peak arises from the signal of nonresonant 2PPE from the Shockley surface state, which partly overlaps with the signal of the $n=1$ image-potential state at the $\bar{\Gamma}$ point for photon energies of 4.82 and 2.41 eV of pump and probe pulses, respectively. The data on Ag(111) show an additional decaying component at negative time delays that can be attributed to the decay of hot electrons excited by the visible pulses and photoemitted by the UV pulses.[50] For positive time delays the population decay can be followed over several orders of magnitude, which makes it possible to determine the inelastic lifetimes of the image-potential states independent of the underlying model to describe the 2PPE process by fitting an exponential decay for positive time delays. Clearly the lifetime of the $n=1$ state increases monotonously with Ar coverage on both surfaces.

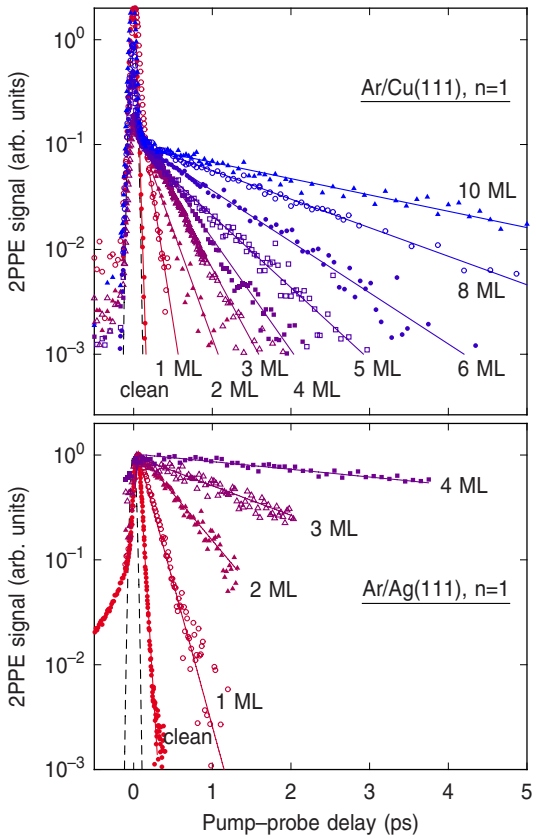

FIG. 6. (Color online) Time-resolved pump-probe traces of the $n=1$ image-potential state at the $\bar{\Gamma}$ point for 0–6, 8, and 10 ML Ar on Cu(111) (top) and 0–4 ML Ar on Ag(111) (bottom). The symbols denote the experimental data whereas the lines show fits of the exponential decay. The black dashed line shows the cross correlation of pump and probe laser pulses determined by nonresonant two-photon photoemission of the Shockley surface state. The data on Ag(111) were normalized to the signal at zero time delay. The data on Cu(111) were normalized to the signal at a time delay of about 200 fs in order to account for the narrow peak from nonresonant 2PPE around zero delay.

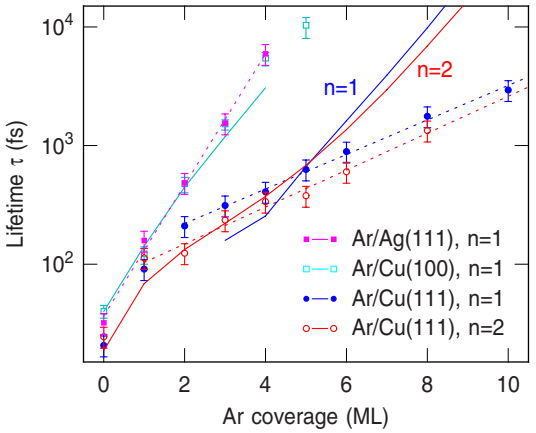

FIG. 7. (Color online) Inelastic lifetimes of the $n=1$ (dots) and $n=2$ (open dots) image-potential states on Ar/Cu(111), and the $n=1$ image-potential state on Ar/Ag(111) (squares) as a function of Ar coverage. The straight dotted lines denote an exponential dependence of the lifetime on Ar coverage. For Ar/Cu(111) the blue and red solid lines (marked by $n=1$ and $n=2$, respectively) depict the results of a model calculation for the elastic decay (see text). The experimental data (open squares) and calculated results (solid line) for the $n=1$ state on Ar/Cu(100) from Ref. 38 are shown in cyan for comparison.

The same behavior has been found for the $n=2$ state on Ar/Cu(111) (not shown).

On the clean Ag(111) surface the lifetimes of the $n=1$ and 2 states have been determined at a temperature of 30 K to 32 and 23 fs, respectively. These values are in excellent agreement with a previous study made at a temperature of 40–50 K.[29] The lifetime of the $n=1$ state rises to about 6 ps at an Ar coverage of 4 ML. On Cu(111) the lifetimes of the $n=1$ and 2 states could be obtained up to an Ar coverage of 10 and 8 ML, respectively. The lifetimes on the clean Cu(111) surface at 26 K have been determined to be 20 and 24 fs for the $n=1$ and 2 states, respectively. The result for the $n=1$ state is in excellent agreement with an earlier study at a similar temperature.[51] Compared to Ag(111) the lifetime of the $n=1$ state on Cu(111) shows a weaker increase with Ar coverage. Up to 10 ML of Ar it does not exceed 3 ps.

V. DISCUSSION

The coverage dependence of the inelastic lifetime (symbols) of all investigated image-potential states is summarized in Fig. 7. Additionally the data for the $n=1$ state on Ar/Cu(100) from Ref. 38 are plotted for comparison. The inelastic lifetime of the $n=1$ state on Ar/Ag(111) shows almost the same exponential increase with the thickness of the Ar adlayers as compared to the $n=1$ state on Ar/Cu(100). Only its absolute value is systematically slightly smaller. The slope of the dotted line that fits very well with the experimental data for Ar/Ag(111) is about 0.55, which means that the lifetime increases by about one order of magnitude every two layers of Ar. This behavior can be understood within the bulk penetration approximation[52] in which the inelastic lifetimes scale inversely to the probability density of the electron inside the metal. This approximation assumes that the decay process is mediated by a local interaction with bulk electrons. It neglects the nonlocal character of the Coulomb interaction, which plays an important role at surfaces due to the reduced screening.[53] It has been shown, however, that the nonlocal contributions to the total decay rate cancel each other to a large extent in favorable cases such as the Cu(100) surface.[54] For Cu(100) the bulk penetration approximation has been successfully used to estimate the change in the inelastic lifetimes of the image-potential states on the quantum number n (Ref. 50) as well as on the thickness of Ar adlayers.[35,40] The latter follows a simple tunneling scheme in which the lifetime increases exponentially with the width of the tunneling barrier formed by the Ar adlayers. The height of the tunneling barrier is essentially given by the energy of the image-potential states relative to the conduction-band minimum E_{CBM} (respectively, the electron affinity $\mathrm{EA}=E_{\mathrm{vac}}-E_{\mathrm{CBM}}$) of the Ar film. The different absolute values of the lifetimes on different metal surfaces, however, can only be explained by realistic many-body calculations that take into account the available phase space for the decay, the different screening of the Coulomb interaction, the nonlocal interac-

tion with the metal electrons, and other effects.[55,56] Therefore, the slope of the exponential increase in the lifetime with coverage should depend within the bulk penetration approximation only on the electronic properties of the adlayer, but not on the metal substrate.

The data for the $n=1$ state on Ar/Cu(111), however, show a completely different behavior. Whereas the initial change in the lifetime with Ar coverage is almost identical as compared to Ar/Ag(111) and Ar/Cu(100), the slope is drastically reduced for coverages $\theta>2$ ML. Just at this coverage the $n=1$ state on Ar/Cu(111) is transformed into an image-potential resonance (cf. Fig. 5). The lifetime of the $n=2$ state, which is resonant to the projected bulk for all Ar coverages, shows the same reduced slope starting from the first monolayer as indicated by the dotted lines, which are exponential fits of the lifetime of $n=1$ and 2 for higher coverages with slopes of 0.15 and 0.16, respectively. The absolute value of the lifetime of $n=2$, however, is systematically smaller by a factor of almost 2 as compared to the $n=1$ state. The reduced slope of the coverage dependence cannot be explained within the tunneling picture. Obviously one expects an overall reduction in the lifetime when an image-potential state is transformed into an image-potential resonance. The decoupling of the wave function and with that the change in the lifetime with coverage of the adlayer should only depend on the properties of the tunnel barrier.

In order to get a deeper understanding of the change in binding energies and lifetimes of the image-potential states and resonances upon Ar adsorption, we have performed model calculations on the basis of the bulk penetration approximation. Wave functions, binding energies, and lifetimes have been computed by numerically solving the stationary Schrödinger equation for the system Ar/Cu(111) using a one-dimensional parametrized model potential that has been successfully used to describe the decoupling of image-potential states by rare-gas layers on Cu(100).[37,40,57] The model potential consists of three parts for the metal, the Ar layer, and vacuum. The metal is represented by a two-band model of nearly-free electrons. The corresponding parameters of the potential have been adjusted to reproduce the size and location of the projected band gap of the Cu(111) surface. The potential inside the Ar layer does not only account for the macroscopic properties of the insulator such as the dielectric constant and the electron affinity, i.e. the location of the conduction-band minimum E_{CBM}, but also for the corrugation of the potential due to the discrete nature of the single layers. The vacuum part is given by the screened image potential.[37]

Solving the stationary Schrödinger equation for different layer thicknesses reveals a single bound state in the vicinity of the vacuum level for coverages $\theta<3$ ML. This state corresponds to the $n=1$ image-potential state. For higher coverages no bound state has been found because the $n=1$ has shifted above the edge of the projected bulk band of the Cu(111) surface. For energies $E>E_{\mathrm{CBM}}$ bulk continuum solutions can be found for all energies within the projected bulk band. These continuum solutions have been normalized with respect to the atomic layer distance in the Cu(111) crystal. Figure 8 shows the probability density integrated over the spatial region in front of the metal surface as a function

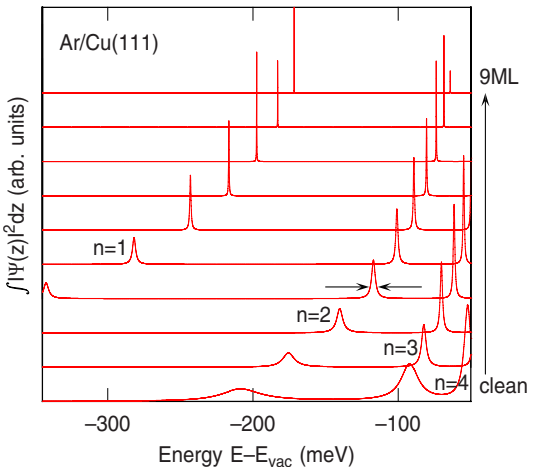

FIG. 8. (Color online) Calculated resonance spectra for different coverages of Ar/Cu(111). The graph shows the integrated probability density of the electron outside the metal as a function of energy. The distinct peaks in these spectra indicate the different image-potential resonances. The widths of the resonances (as indicated by the arrows) are assumed to scale inversely with the (elastic) lifetime.

of energy for 0–9 ML of Ar/Cu(111). This value corresponds to the probability for an electron to reside in the vacuum. The resonance spectra for all coverages show distinct peaks. With increasing Ar coverage their widths become narrower and their peak intensity increases while they shift to higher energies. The positions of the peaks can be directly identified as the binding energy of the image-potential resonances of this system. The widths of the peaks depend on the coupling of the resonance to the continuum of bulk states and thus are a measure of the probability for elastic decay, i.e., for the rate of elastic charge transfer of an electron excited in front of the surface into the metal bulk. Therefore, we assume that the elastic lifetimes τ of the resonances scale inversely with their width ΔE (FWHM) as $\tau=\hbar/\Delta E$, where $\hbar$ is the Planck constant divided by 2π.

The results for the calculated binding energies of the $n=1$ and 2 image-potential resonances on Ar/Cu(111) are shown as lines in Fig. 9 together with the experimental data (symbols). The calculated and experimental energies show a very good agreement although the model potential has no free parameters. The largest deviation is found on the clean surface where the simulation overestimates the binding energy for the $n=1$ as well as for the $n=2$ state. For higher coverages the numerical values for the $n=2$ fit nearly perfectly with the experimental data. In the case of the $n=1$ state the model calculation also underestimates the experimental data for 1 and 2 ML coverage, but shows a better agreement for higher coverages.

The calculated elastic lifetimes for the $n=1$ and $n=2$ states are shown as solid lines (marked by $n=1$ and $n=2$, respectively) in comparison with the experimental data in Fig. 7. For coverages below 5 ML the agreement between model and experiment for the $n=1$ as well as for the $n=2$ resonance is reasonable. For these coverages the results of the model calculation slightly underestimate the lifetimes even though the model does not include inelastic decay. One

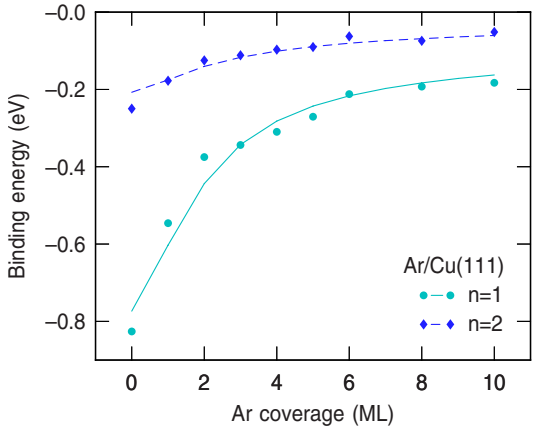

FIG. 9. (Color online) Comparison of measured and calculated binding energies of the $n=1$ (dots) and $n=2$ (diamonds) for Ar/Cu(111). Experimental values are shown as symbols; the results of the calculations on the basis of a one-dimensional model potential are drawn as lines.

reason for this might be that the parameters of the used potential have been adjusted to reproduce the correct binding energies.[37,58] The linewidths and therefore the lifetimes, however, depend sensitively on the detailed form of the wave functions. Note that the model is not applicable for the $n=1$ state as long as it is a bound state or its energy is very close to the edge of the projected bulk band, which is the case for coverage below 3 ML. For coverages above 5 ML, however, the model calculations obviously overestimate the lifetimes compared to the experimental data. The change in the calculated elastic lifetime on Ar coverage, i.e. the slope, in this range is comparable with the change observe for Ar/Ag(111) and Ar/Cu(100) as expected from the simple tunneling picture mentioned above in which the change in the lifetime only depends on the width of the tunneling barrier. The experimental lifetimes for Ar/Cu(111), however, show a much smaller change on Ar coverage. This cannot be explained by the neglect of the inelastic decay in the model calculation since in particular at large coverages where the decoupling is strong it cannot be expected that the contribution of the inelastic decay rate to the total decay rate increases with increasing coverage.

At this point we see basically two different arguments to explain the obvious discrepancy between the experimental and theoretical dependences of the lifetimes of the image-potential resonance on Ar coverage. On one hand one could imply that the quality or the effective thickness of the Ar layers is smaller than expected. In particular the last point would lead to a reduced decoupling and therefore to a shorter lifetime of the image-potential resonances. It is, however, very unlikely that the morphology of physisorbed Ar layers on Cu(111) is very different from Ar layers on Ag(111) and Cu(100), which have been prepared using exactly the same procedure. This is proven by the fact that the TPD spectra (Fig. 1) are almost identical for Ar on Cu(111) and Ag(111) and indicate the growth of well-ordered Ar layers.

On the other hand, one has to consider the shortcoming of the applied theoretical model. The wave functions we use to calculate resonance spectra are the results of solving the stationary Schrödinger equation and are thus eigenstates of the system. When we compare the results of these calculations with the time-resolved photoemission experiment, we implicitly assume that the transient population that the pump pulse creates and that the probe pulse photoemits can be described in terms of these eigenstates. This may be a good approximation in cases when a gap in the projected bulk band structure confines the eigenstates to the surface but not in the presence of continuum states in the bulk. In that case, the stationary state is, strictly speaking, neither reached nor probed in a situation when the initial excitation and the final photoemission processes takes place in a narrow region near the surface. A realistic calculation of the dynamical process of the 2PPE experiment would perhaps have to start with an electron wave packet in the ground state and consider its excitation with the pump pulse, its subsequent propagation in space, and finally its photoemission into the vacuum. The fact that the image potential itself is not a ground-state property of the surface, but the result of a dynamical screening of the excited electron, is probably negligible for the time scales of the present experiment.

VI. CONCLUSIONS

Time-resolved 2PPE has been applied to study the transition of an image-potential state to a resonance on Cu(111). Well-ordered Ar spacer layers were used to decouple the image states from the metal surface. On the clean Cu(111) surface the first $(n=1)$ image-potential state is located close below the projected bulk band. The reduction in the binding energy due to the adsorption of Ar adlayers shifts the $n=1$ state above the minimum of the unoccupied projected bulk band of Cu(111) and thus induces a transition from an image-potential state to a resonance. As a consequence, a strikingly different dependence of the inelastic lifetime of the $n=1$ state on Ar layer thickness is observed on Cu(111) as compared to Ag(111) as well as compared to previous results on Cu(100).[35] On Ag(111) the lifetime shows a continuous exponential increase with the layer thickness and reaches about 6 ps at an Ar coverage of 4 ML. The thickness dependence of the lifetime on this surface is comparable to the results on Cu(100). The initial increase in the lifetime with the layer thickness on Cu(111) is essentially the same as compared to Ag(111) and Cu(100). However, this exponential increase is considerably reduced when the $n=1$ state becomes a resonance. Up to 10 ML of Ar the lifetime on Cu(111) does not exceed 3 ps. This behavior cannot be explained within a tunneling picture in which the decoupling of the image-potential states depends only on the tunnel barrier formed by the Ar layers nor by calculations based on a model potential that includes the projected electronic band structure of Cu(111) as well as the dielectric properties and the corrugated structure of the Ar adlayers.

ACKNOWLEDGMENTS

We thank F. Rebentrost for his help with the numerical simulations of our data and acknowledge funding by the Deutsche Forschungsgemeinschaft through Grant No. HO 2295/1 and No. GK 790.

[1] H. Petek, M. J. Weida, H. Nagano, and S. Ogawa, Science **288**, 1402 (2000).
[2] A. D. Miller, I. Bezel, K. J. Gaffney, S. Garrett-Roe, S. H. Liu, P. Szymanski, and C. B. Harris, Science **297**, 1163 (2002).
[3] C. Gahl, U. Bovensiepen, C. Frischkorn, and M. Wolf, Phys. Rev. Lett. **89**, 107402 (2002).
[4] M. Weinelt, M. Kutschera, T. Fauster, and M. Rohlfing, Phys. Rev. Lett. **92**, 126801 (2004).
[5] X. Y. Zhu, Surf. Sci. Rep. **56**, 1 (2004).
[6] B. Li, J. Zhao, K. Onda, K. D. Jordan, J. L. Yang, and H. Petek, Science **311**, 1436 (2006).
[7] J. Güdde, M. Rohleder, T. Meier, S. W. Koch, and U. Höfer, Science **318**, 1287 (2007).
[8] C. H. Schwalb, S. Sachs, M. Marks, A. Schöll, F. Reinert, E. Umbach, and U. Höfer, Phys. Rev. Lett. **101**, 146801 (2008).
[9] F. Schmitt, P. S. Kirchmann, U. Bovensiepen, R. G. Moore, L. Rettig, M. Krenz, J.-H. Chu, N. Ru, L. Perfetti, D. H. Lu, M. Wolf, I. R. Fisher, and Z.-X. Shen, Science **321**, 1649 (2008).
[10] M. Cinchetti, K. Heimer, J. Wüstenberg, O. Andreyev, M. Bauer, S. Lach, C. Ziegler, Y. Gao, and M. Aeschlimann, Nature Mater. **10**, 1 (2008).
[11] T. Ichibayashi and K. Tanimura, Phys. Rev. Lett. **102**, 087403 (2009).
[12] U. Höfer, I. L. Shumay, C. Reuß, U. Thomann, W. Wallauer, and T. Fauster, Science **277**, 1480 (1997).
[13] W. Berthold, U. Höfer, P. Feulner, E. V. Chulkov, V. M. Silkin, and P. M. Echenique, Phys. Rev. Lett. **88**, 056805 (2002).
[14] M. Weinelt, J. Phys.: Condens. Matter **14**, R1099 (2002).
[15] P. M. Echenique, R. Berndt, E. V. Chulkov, T. Fauster, A. Goldmann, and U. Höfer, Surf. Sci. Rep. **52**, 219 (2004).
[16] W. Berthold, J. Güdde, P. Feulner, and U. Höfer, Appl. Phys. B: Lasers Opt. **73**, 865 (2001).
[17] K. Boger, M. Weinelt, and T. Fauster, Phys. Rev. Lett. **92**, 126803 (2004).
[18] T. Fauster, M. Weinelt, and U. Höfer, Prog. Surf. Sci. **82**, 224 (2007).
[19] M. Rohleder, W. Berthold, J. Güdde, and U. Höfer, Phys. Rev. Lett. **94**, 017401 (2005).
[20] A. B. Schmidt, M. Pickel, M. Wiemhofer, M. Donath, and M. Weinelt, Phys. Rev. Lett. **95**, 107402 (2005).
[21] A. Winkelmann, F. Bisio, R. Ocana, W. C. Lin, M. Nyvlt, H. Petek, and J. Kirschner, Phys. Rev. Lett. **98**, 226601 (2007).
[22] P. M. Echenique and J. B. Pendry, J. Phys. C **11**, 2065 (1978).
[23] M. Bauer, S. Pawlik, and M. Aeschlimann, Phys. Rev. B **55**, 10040 (1997).
[24] H. Petek and S. Ogawa, Annu. Rev. Phys. Chem. **53**, 507 (2002).
[25] A. G. Borisov, J. P. Gauyacq, A. K. Kazansky, E. V. Chulkov, V. M. Silkin, and P. M. Echenique, Phys. Rev. Lett. **86**, 488 (2001).
[26] A. Föhlisch, P. Feulner, F. Hennies, A. Fink, D. Menzel, D. Sanchez-Portal, P. M. Echenique, and W. Wurth, Nature (London) **436**, 373 (2005).
[27] D. F. Padowitz, W. R. Merry, R. E. Jordan, and C. B. Harris, Phys. Rev. Lett. **69**, 3583 (1992).
[28] X. Y. Zhu, Annu. Rev. Phys. Chem. **53**, 221 (2002).
[29] R. L. Lingle, N. H. Ge, R. E. Jordan, J. D. McNeill, and C. B. Harris, Chem. Phys. **205**, 191 (1996).
[30] N. H. Ge, C. M. Wong, and C. B. Harris, Acc. Chem. Res. **33**, 111 (2000).
[31] A. Hotzel, G. Moos, K. Ishioka, M. Wolf, and G. Ertl, Appl. Phys. B: Lasers Opt. **68**, 615 (1999).
[32] J. D. McNeill, R. L. Lingle, R. E. Jordan, D. F. Padowitz, and C. B. Harris, J. Chem. Phys. **105**, 3883 (1996).
[33] M. Wolf, E. Knoesel, and T. Hertel, Phys. Rev. B **54**, R5295 (1996).
[34] W. Berthold, U. Höfer, P. Feulner, and D. Menzel, Chem. Phys. **251**, 123 (2000).
[35] W. Berthold, P. Feulner, and U. Höfer, Chem. Phys. Lett. **358**, 502 (2002).
[36] M. Machado, E. V. Chulkov, V. M. Silkin, U. Höfer, and P. M. Echenique, Prog. Surf. Sci. **74**, 219 (2003).
[37] W. Berthold, F. Rebentrost, P. Feulner, and U. Höfer, Appl. Phys. A: Mater. Sci. Process. **78**, 131 (2004).
[38] D. C. Marinica, C. Ramseyer, A. G. Borisov, D. Teillet-Billy, J. P. Gauyacq, W. Berthold, P. Feulner, and U. Höfer, Phys. Rev. Lett. **89**, 046802 (2002).
[39] M. Machado, W. Berthold, U. Höfer, E. V. Chulkov, and P. M. Echenique, Surf. Sci. **564**, 87 (2004).
[40] J. Güdde and U. Höfer, Prog. Surf. Sci. **80**, 49 (2005).
[41] C. Reuß, I. L. Shumay, U. Thomann, M. Kutschera, M. Weinelt, T. Fauster, and U. Höfer, Phys. Rev. Lett. **82**, 153 (1999).
[42] M. Rohleder, K. Duncker, W. Berthold, J. Güdde, and U. Höfer, New J. Phys. **7**, 103 (2005).
[43] H. Schlichting and D. Menzel, Surf. Sci. **285**, 209 (1993).
[44] K. Giesen, F. Hage, F. J. Himpsel, H. J. Riess, and W. Steinmann, Phys. Rev. B **33**, 5241 (1986).
[45] F. Reinert, G. Nicolay, S. Schmidt, D. Ehm, and S. Hüfner, Phys. Rev. B **63**, 115415 (2001).
[46] F. Forster, S. Hüfner, and F. Reinert, J. Phys. Chem. B **108**, 14692 (2004).
[47] Q. Zhong, C. Gahl, and M. Wolf, Surf. Sci. **496**, 21 (2002).
[48] M. Marks, K. Schubert, C. H. Schwalb, and U. Höfer (unpublished).
[49] W. Berthold, P. Feulner, and U. Höfer, Surf. Sci. **548**, L13 (2004).
[50] I. L. Shumay, U. Höfer, C. Reuß, U. Thomann, W. Wallauer, and T. Fauster, Phys. Rev. B **58**, 13974 (1998).
[51] E. Knoesel, A. Hotzel, and M. Wolf, J. Electron Spectrosc. Relat. Phenom. **88-91**, 577 (1998).
[52] T. Fauster and W. Steinmann, in *Electromagnetic Waves: Recent Developments in Research*, edited by P. Halevi (North-Holland, Amsterdam, 1995), Vol. 2, pp. 347–411.
[53] P. M. Echenique, J. M. Pitarke, E. V. Chulkov, and A. Rubio, Chem. Phys. **251**, 1 (2000).
[54] E. V. Chulkov, I. Sarria, V. M. Silkin, J. M. Pitarke, and P. M. Echenique, Phys. Rev. Lett. **80**, 4947 (1998).
[55] I. Sarria, J. Osma, E. V. Chulkov, J. M. Pitarke, and P. M. Echenique, Phys. Rev. B **60**, 11795 (1999).
[56] A. Garcia-Lekue, J. M. Pitarke, E. V. Chulkov, A. Liebsch, and P. M. Echenique, Phys. Rev. B **68**, 045103 (2003).
[57] M. Rohleder, K. Duncker, W. Berthold, J. Güdde, and U. Höfer, Appl. Phys. A: Mater. Sci. Process. **88**, 527 (2007).
[58] E. V. Chulkov, V. M. Silkin, and P. M. Echenique, Surf. Sci. **437**, 330 (1999).